Matrix stiffness reverses the effect of actomyosin tension on cell proliferation

Justin D. Mih, Aleksandar Marinkovic, Fei Liu, Asma S. Sharif and Daniel J. Tschumperlin*

Molecular and Integrative Physiological Sciences, Department of Environmental Health, Harvard School of Public Health, Boston, MA 02115, USA

*Author for correspondence (dtschump@hsph.harvard.edu)

Accepted 14 October 2012
Journal of Cell Science 125, 5974–5983

doi: 10.1242/jcs.108886

Summary

The stiffness of the extracellular matrix exerts powerful effects on cell proliferation and differentiation, but the mechanisms transducing matrix stiffness into cellular fate decisions remain poorly understood. Two widely reported responses to matrix stiffening are increases in actomyosin contractility and cell proliferation. To delineate their relationship, we modulated cytoskeletal tension in cells grown across a physiological range of matrix stiffnesses. On both synthetic and naturally derived soft matrices, and across a panel of cell types, we observed a striking reversal of the effect of inhibiting actomyosin contractility, switching from the attenuation of proliferation on rigid substrates to the robust promotion of proliferation on soft matrices. Inhibiting contractility on soft matrices decoupled proliferation from cytoskeletal tension and focal adhesion organization, but not from cell spread area. Our results demonstrate that matrix stiffness and actomyosin contractility converge on cell spreading in an unexpected fashion to control a key aspect of cell fate.

Key words: Actomyosin tension, Cell proliferation, Matrix stiffness

Introduction

Cells adhered to a rigid substrate, such as a petri dish, typically assemble well-organized actin networks that associate with myosin to form contractile stress fibers (Cai et al., 2006; Hotulainen and Lappalainen, 2006). These cytoskeletal elements terminate at focal adhesions that link the cytoskeleton to the extracellular matrix via integrins (Geiger et al., 2009). In spread cells, inhibition of RhoA or interference with actomyosin contractility results in the disassembly of stress fibers and focal adhesions, along with broad inhibition of cell proliferation (Assoian and Klein, 2008; Chicurel et al., 1998; Mammoto and Ingber, 2009; Provenzano and Keely, 2011; Straight et al., 2003; Wozniak and Chen, 2009).

Cell spreading is tightly coupled to proliferation (Folkman and Moscona, 1978; Chen et al., 1997). Restricting the spread area of adherent cells can lead to growth arrest, but as the spread area increases, so does proliferation. Cell traction forces and RhoA activity also increase with cell spreading (Califano and Reinhart-King, 2010; McBeath et al., 2004; Tolić-Nørrelykke et al., 2005; Wang et al., 2002) reinforcing the idea that elevated actomyosin tension promotes cell cycle progression (Huang et al., 1998).

Cell spreading is also controlled by extracellular matrix stiffness. When grown on soft matrices, many cell types exhibit less spreading, as well as reductions in proliferation, traction forces, stress fibers, and focal adhesions (Aratyn-Schaus and Gardel, 2010; Califano and Reinhart-King, 2010; Chowdhury et al., 2010; Fringer and Grinnell, 2001; Fu et al., 2010; Georges and Janmey, 2005; Ghosh et al., 2007; Kong et al., 2005; Levental et al., 2009; Lo et al., 2000; Paszek et al., 2005; Rhee et al., 2007; Saez et al., 2005; Solon et al., 2007; Wozniak et al., 2003). These observations, which recapitulate the effects of reducing cytoskeletal tension in spread cells, suggest that insufficient actomyosin-based contractility may underlie the suppression of cell proliferation on soft matrices. Yet, it has also been shown in some cases that actomyosin contractility is not predictive of cell proliferation (Roca-Cusachs et al., 2008) and that inhibition of Rho-associated protein kinase (ROCK) partially rescues rounded endothelial cells from G1 arrest (Mammoto et al., 2004). In fact, inhibition of nonmuscle myosin II in fibroblasts grown on a physiologically soft matrix rescues their proliferation to levels attained on rigid substrates (Mih et al., 2011). This raises a mystery as to why inhibition of myosin in such contexts should exert such a profound stimulatory effect on cell proliferation, and whether our understanding of tensional control of growth, gleaned mostly from studies on rigid substrates, is incomplete.

Here we examine the relationship between cell tension and proliferation across matrices of varying stiffness, and in doing so, attempt to shed light on why soft matrix environments generally suppress the proliferation of adherent cells. Although we confirm that fibroblasts on soft matrices generate lower contractile forces than on rigid matrices, our data demonstrate that inhibition of actomyosin contractility selectively promotes cell proliferation on soft matrices, suggesting that in such contexts, cell-generated forces act as a brake against proliferation. Moreover, we show that cell spreading and proliferation are tightly coupled, even across large variations in matrix stiffness and contractile force generation. Based on these observations, we propose that the ‘excessive’ generation of contractile forces against insufficiently stable cell-matrix adhesions underlies the restriction of cell spreading and proliferation on soft matrices.

Results

To delineate the combined effects of matrix stiffness and modulation of actomyosin contractile function on cell proliferation, we synthesized polyacrylamide (PA) hydrogels of

defined stiffness within 96-well glass-bottom plates (Mih et al., 2011). The gels were functionalized with monomeric collagen I at a constant density across all stiffness conditions, allowing for the isolation of matrix stiffness effects. Using this system, we compared cell growth on collagen I-coated rigid (glass) versus relatively soft, physiologically relevant PA gels (1 kPa elastic [Young's] modulus) (Discher et al., 2005; Klein et al., 2009; Liu et al., 2010; Paszek et al., 2005), and confirmed that inhibition of myosin II with blebbistatin evoked divergent dose-dependent effects on cell number (Fig. 1A), enhancing proliferation on a soft matrix while inhibiting proliferation on glass (Mih et al., 2011). We documented a similar trend of increasing BrdU incorporation, indicative of ongoing DNA synthesis, when blebbistatin was applied to cells on 0.3 and 1 kPa gels, and decreasing BrdU incorporation when blebbistatin was applied on rigid surfaces (Fig. 1B). We next applied inhibitors of Rho and ROCK, which are upstream controllers of actomyosin contractile function, to fibroblasts cultured on glass and 1 kPa gels. Similarly divergent stiffness-dependent effects on cell proliferation were observed with each of these treatments, including the Rho antagonist C3 transferase and two ROCK inhibitors, Y27632 and GSK429286 (Fig. 1C). While the analogous results across a panel of independent treatments were indicative of on-target effects, to directly link the divergent responses to myosin inactivation we employed siRNA targeting non-muscle myosin heavy chain IIa (MYH9). Blots confirming the efficacy of siRNA knockdown are included in the supplementary material (supplementary material Fig. S1). Across a range of siRNA concentrations (0.005–50 nM), we found that partial MYH9 knockdown (0.5 nM) exerted divergent effects on cell proliferation between glass and 1 kPa gels (Fig. 1D), recapitulating the small molecule inhibitor results.

To confirm that the divergent effects of Rho–ROCK–myosin inhibition reflected a bona fide influence of matrix stiffness, we applied a single dose of selected inhibitors to fibroblasts cultured on 0.3, 1, 6, 20 kPa gels and glass (Fig. 1E). In all cases, the proliferation-promoting effects of inhibiting actomyosin tension were reproduced on the softest matrices, and gradually dissipated or reversed as matrix stiffness increased, establishing that the conditional nature of Rho–ROCK–myosin effect on cell proliferation is a function of underlying matrix stiffness.

Extending these observations to other cell types, we found that the divergent matrix stiffness-dependent effects of ROCK inhibition were broadly, though not universally, conserved across a panel of primary and transformed cell lines (Fig. 1F). Primary low passage fibroblasts from human lungs (NHLF), as well as primary human bone marrow-derived (hMSC) and adipose-derived mesenchymal stem cells (hASC), all recapitulated the stiffness-dependent effects of ROCK inhibition. Similarly, IMR-90 and NIH3T3 fibroblast cell lines demonstrated divergent stiffness-dependent responses, as did the RLE6TN rat lung epithelial cell line. In contrast, A549 and MDCKII epithelial cell lines exhibited little response to ROCK inhibition on stiff substrates, with relatively muted increases in cell number on 1 kPa gels. Intriguingly, the breast cancer derived MDA-MB-231 cell line was the most sensitive in our panel to growth inhibition on a stiff matrix, and was the only line that did not increase its growth on 1 kPa gels upon ROCK inhibition. While the panel of cell types tested here is far from exhaustive, the aggregate results point toward a potentially broad relevance of stiffness-dependent actomyosin effects, particularly among non-transformed mesenchymal cell types.

We also applied ROCK inhibitor treatments to fibroblasts growing within three-dimensional Geltrex matrices, which are derived from the basement membrane of Engelbreth–Holm–Swarm tumor cells and have mechanical properties in the range of softest PA gels used above. Similar to our observations on soft, synthetic 2D matrices, we confirmed that Y27632 and GSK429286 stimulated fibroblast proliferation within these soft, biologically derived 3D matrices (Fig. 1G), switching from a net loss in cell number in the absence of inhibitors to a net gain of cells with ROCK inhibition.

Based on the considerable evidence positively linking cell proliferation to focal adhesions and actomyosin force generation (Assoian and Klein, 2008; Huang and Ingber, 1999; Mammoto and Ingber, 2009; Provenzano and Keely, 2011; Wozniak and Chen, 2009), we first suspected that inhibition of Rho, ROCK, and myosin might be exerting unanticipated effects on these structural and functional features when applied to cells growing on soft matrices. We began by measuring each of these features and their variation across matrix stiffness under baseline culture conditions. We found that increasing matrix stiffness promotes a subtle increase in staining for phosphorylated myosin light chain (Fig. 2A), and a gradual rise in cellular force generation with increasing matrix stiffness (Fig. 2B), as measured by Fourier transform traction microscopy (Butler et al., 2002; Marinković et al., 2012). As expected, increasing matrix stiffness also enhances the organization of increasingly large islands of adhesion proteins, visualized by vinculin (Fig. 2D) and talin (Fig. 2E) immunostaining and quantified by mean focal adhesion length (Fig. 2F). These trends are consistent with prior observations (Califano and Reinhart-King, 2010; Chowdhury et al., 2010; Fu et al., 2010; Ghosh et al., 2007; Kong et al., 2005; Lo et al., 2000; Paszek et al., 2005; Saez et al., 2005).

When we treated cells with the ROCK inhibitor Y27632, all of these structural and functional readouts changed as expected, without any unusual variation across matrix stiffness conditions. That is, ROCK inhibition attenuated myosin light chain phosphorylation (Fig. 2A) and reduced cell tractions by more than 50% in every condition (Fig. 2B), indicating a loss of cytoskeletal tension and effectively decoupling cell tractions from proliferation (Fig. 2C). Similarly, vinculin and talin staining was reduced by ROCK inhibition on stiff PA gels (Fig. 2D,E), and focal adhesions remained small or undetectable on soft PA gels (Fig. 2F). Therefore, while all of these features naturally vary across matrix stiffness, and in all cases correlate with baseline cell proliferation, our observation that ROCK inhibition on soft matrices stimulates cell proliferation, while each of these features is suppressed or remains absent, indicates that they do not positively regulate matrix stiffness-dependent control of proliferation.

To ascertain how actomyosin tension might act to inhibit cell proliferation on soft matrices, we first noted that at baseline, cells on highly compliant matrices ($<$1 kPa) exhibit a rounded morphology (Fig. 3A). Although cells on soft substrates tend to interact more with each other and form colonies (Guo et al., 2006), here fibroblasts were seeded sparsely and remained well distributed (Fig. 3A), arguing against contact-inhibition as the primary restraint against proliferation. Strikingly, inhibition of ROCK or myosin II engaged cell spreading on these soft matrices (Fig. 3A), consistent with observations that inhibition of NMM-II

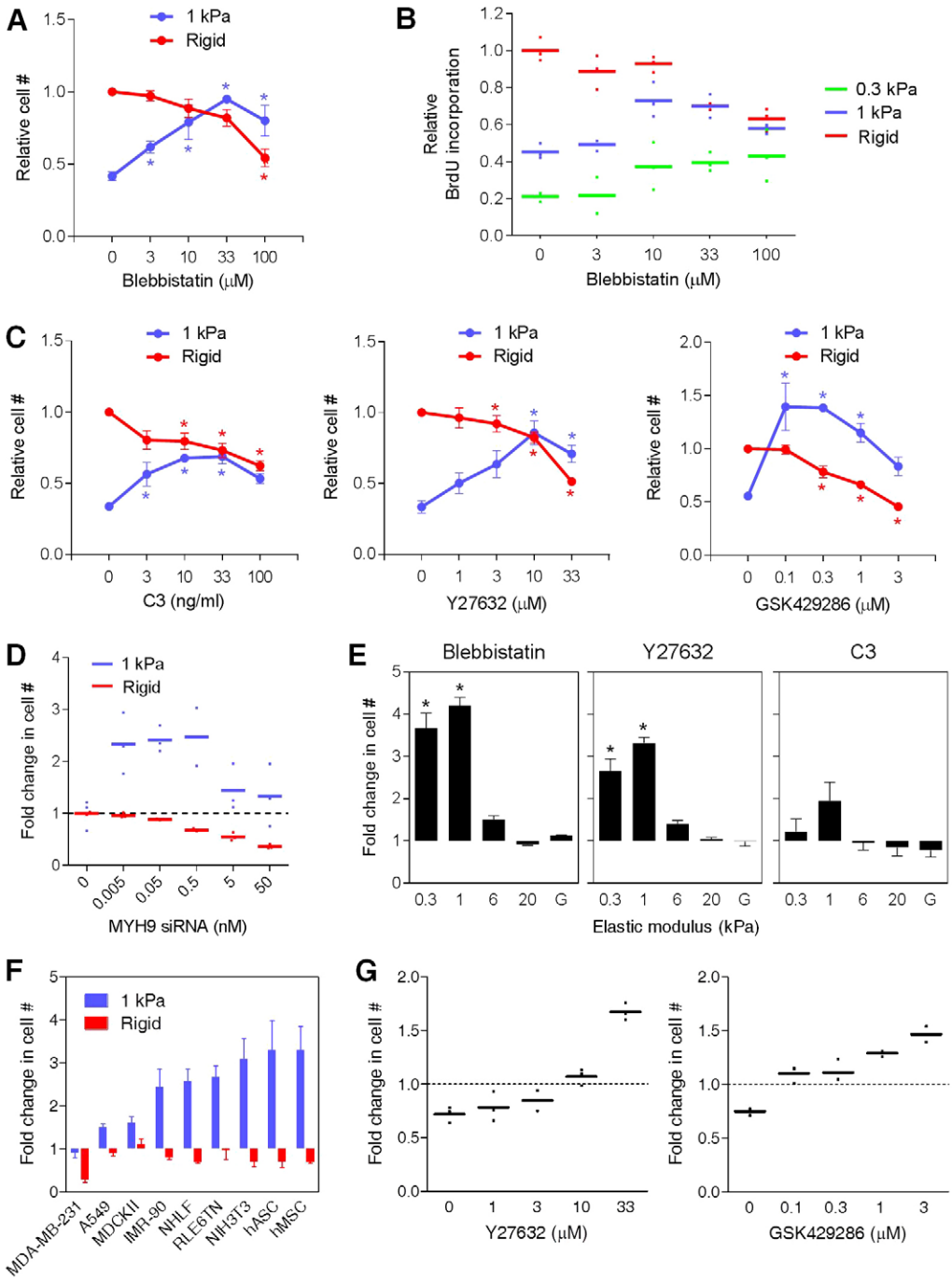

Fig. 1. Inhibition of Rho–ROCK–myosin switches from suppression to promotion of cell proliferation as matrix stiffness decreases. (**A**) Lung fibroblasts were seeded on collagen I-coated 1 kPa and rigid (glass) substrates at low density and cultured in the presence of various concentrations of blebbistatin for 72 hours. Cell numbers are normalized to the rigid, no drug condition. Data are means ± s.e.m. (n=3). One-way ANOVA followed by Tukey's test: *P<0.05 versus no drug for the same stiffness condition. (**B**) BrdU incorporation over 48 hours normalized to the no drug, rigid condition. Means and individual data points from one experiment are shown. (**C**) Fibroblasts were treated with C3 transferase and two ROCK inhibitors for 72 hours. Data are means ± s.e.m. (n≥3). One-way ANOVA followed by Tukey's test: *P<0.05 versus no drug for the same stiffness condition. (**D**) Fibroblasts on 1 kPa and rigid substrates were transfected with different concentrations of siRNA targeting MYH9 and cultured for 6 days. Fold change in cell number is normalized against a concentration-matched negative siRNA control for each stiffness condition. Means and individual data points from one experiment are shown. (**E**) Effects of blebbistatin (10 μM), Y27632 (10 μM), and C3 transferase (100 ng/ml) on cell proliferation across five stiffness conditions. Fold change indicates ratio of cell number in the drug versus no drug condition after 72 hours. Data are means ± s.e.m. (n=3). One-way ANOVA followed by Tukey's test: *P<0.0001 versus rigid (G, glass) condition. (**F**) Effect of GSK429286 (1 μM) on a panel of normal and immortalized cell types cultured on 1 kPa and rigid substrates. Fold change represents cell number in the drug versus no drug condition following 72 hours of exposure. MDA-MB-231, breast cancer cell line; A549, human lung adenocarcinoma cell line; MDCKII, Madin–Darby canine kidney epithelial cell line; IMR-90, normal human fetal lung fibroblast; NHLF, normal human adult lung fibroblast; RLE6TN, rat lung epithelial cell line; NIH3T3, mouse embryonic fibroblast cell line; hASC, human adipose-derived stem cells; hMSC, human bone marrow-derived stem cells. Data are means ± s.d. (n=3). (**G**) Lung fibroblasts were seeded within Geltrex 3D matrices and exposed to Y27632 (10 μM) or GSK429286 (1 μM). Fold change represents cell number after 5 days versus an initial 4 hour time point. Means and individual data points from one experiment are shown.

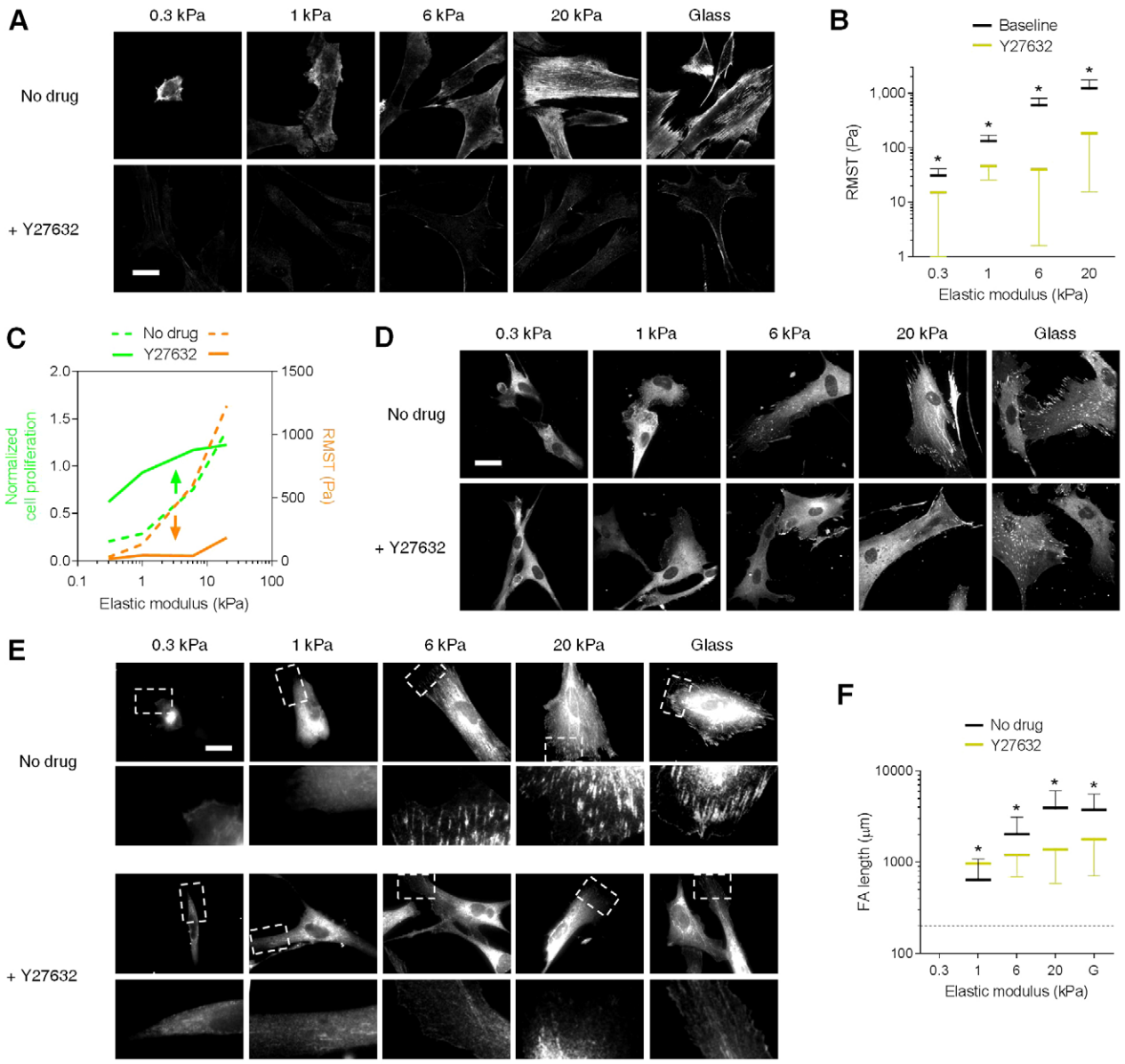

Fig. 2. Proliferation on soft matrices is decoupled from myosin light chain phosphorylation, cell tractions, and focal adhesions. (**A**) Immunofluorescence staining of phosphorylated myosin light chain in fibroblasts across matrix stiffness. Y27632 (10 μM) was applied for 24 hours. (**B**) Fibroblast root-mean-square tractions (RMST) measured by Fourier transform traction microscopy. Y27632 (10 μM) was applied for 45 minutes. Means and data points ($n=5$ cells) are shown. Student's *t*-test: $^*P<0.0001$ versus no drug. (**C**) Relationship between cell proliferation and tractions with or without Y27632 (10 μM). Proliferation is expressed as cell number relative to the no drug, rigid condition following 72 hours of culture of one representative experiment. (**D**,**E**) Immunofluorescence staining of vinculin (D) and talin (E) across matrix stiffness. Images are at 400× magnification; corresponding images of boxed regions are at 1000×. Scale bar: 25 μm. (**F**) Effect of matrix stiffness and Y27632 (10 μM) on focal adhesion (FA) length. Focal adhesions on 0.3 kPa gels were not observed above the detection threshold (0.2 μm). Data are means ± s.d. ($n\geq47$). Student's *t*-test: $^*P<0.001$ versus no drug.

causes some adherent cell types to appear more dendritic (Straight et al., 2003) and rescues the spreading and motility of glial cells on highly compliant substrates (Ulrich et al., 2009). Quantifying this spreading effect in cell populations across matrix stiffness conditions, we observed an increase in 2D projected cell area after ROCK inhibition on soft PA gels (Fig. 3B). This area change exceeded that which would be expected from relaxation of cell contraction alone, consistent with initiation of an active cell spreading process upon ROCK inhibition. At baseline, we found that 2D cell area tracked with matrix stiffness up to a plateau at 20 kPa (Fig. 3B), and was well correlated with the effect of matrix stiffness on cell proliferation. ROCK inhibition induced dramatic cell spreading on soft matrices, up to 10-fold on 0.3 kPa substrates, while evoking comparably little effect on stiff matrices (Fig. 3B). Simultaneous knockdown of ROCK1 and ROCK2 with siRNA also enhanced cell spreading on soft matrices (Fig. 3C) and recapitulated the divergent effects of ROCK inhibitors on cell proliferation between glass and 1 kPa gels (Fig. 3D) and across a range of stiffness conditions (Fig. 3E). When we plotted cell proliferation

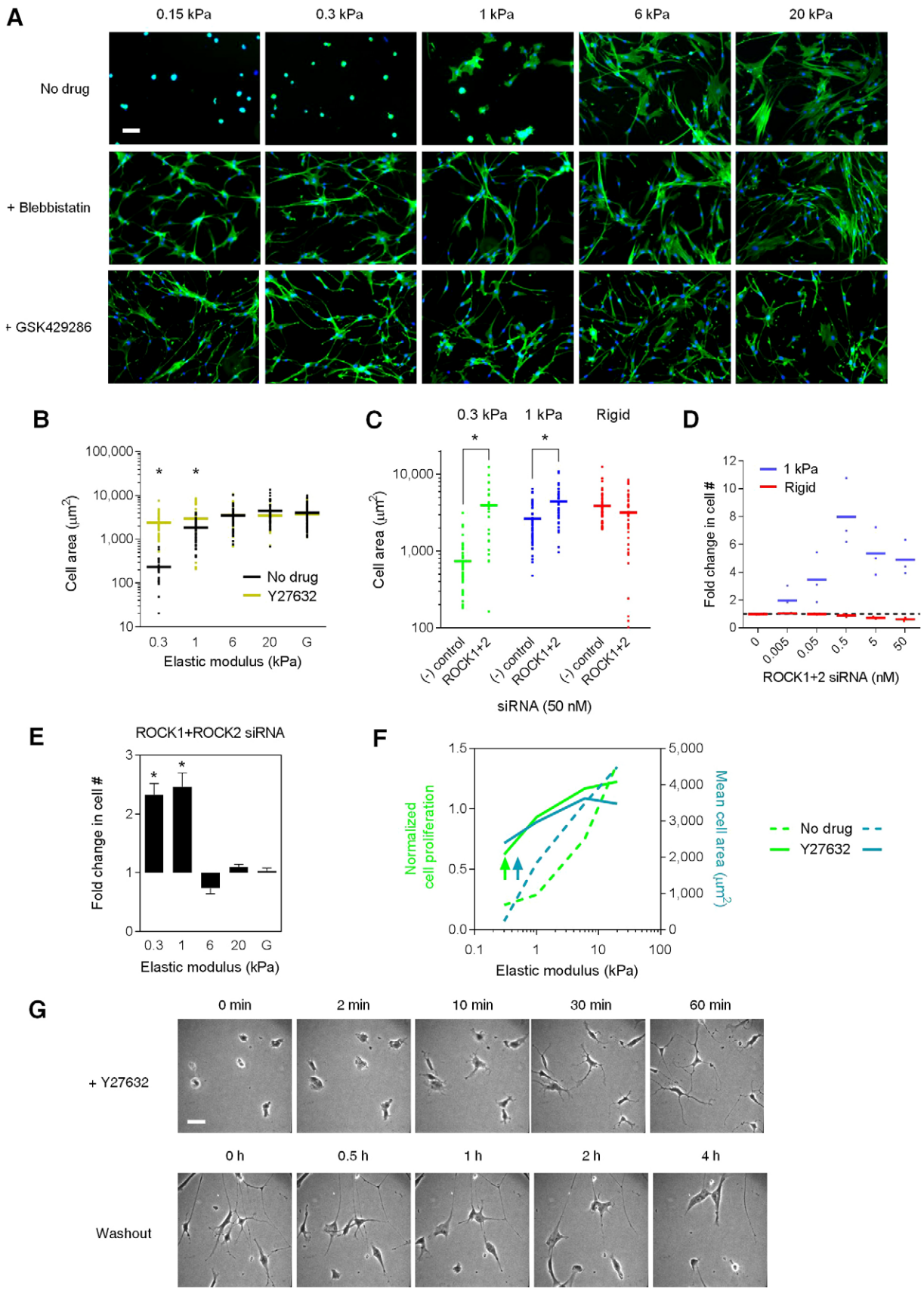

Fig. 3. See next page for legend.

and cell area across matrix stiffness both with and without Y27632 treatment, these features remained tightly correlated (Fig. 3F), in contrast with the lack of a positive correlation with cell tractions (Fig. 2C).

Time-lapse imaging provided dramatic confirmation of the morphological effects of ROCK inhibition on individual cells cultured on soft matrices (Fig. 3G; supplementary material Movie 1). Upon treatment, cells quickly transitioned from small, roughly round shapes to the extension of prominent dendrite-like projections not unlike those observed in fibroblasts spreading within soft 3D hydrogels (Grinnell et al., 2003; Rhee et al., 2007). This response is analogous to the increase in proplatelet extensions that occurs upon inhibition of myosin II in megakaryocytes (Shin et al., 2011), which was also reported to generate an increase in MK polyploidy. Although we did not observe any multinucleation in the fibroblasts tested here, it is notable that in both contexts inhibition of myosin II leads to increased DNA replication. The transition in cell morphology induced by ROCK inhibition was reversible, as visualized upon washout of Y27632 (Fig. 3G; supplementary material Movie 2), emphasizing the plasticity of cell spreading on soft substrates and the dynamic and transient nature of cell–matrix adhesions formed upon ROCK inhibition.

If an excess of endogenous actomyosin tension is responsible for impaired spreading and proliferation on soft matrices, then the enhancement of actomyosin tension on relatively soft matrices should further reduce cell spreading and proliferation. Consistent with this hypothesis, we previously observed that the small molecule cantharidin, which increases contractility through inhibition of protein phosphatase I (Knapp et al., 1998), suppresses the proliferation of cells on 1 kPa gels but not on glass substrates (Mih et al., 2011). Here we verified that the effect of cantharidin (1 μM) was dependent on matrix stiffness (Fig. 4A). Using traction force microscopy, we found that cantharidin evoked a modest but significant increase in cell tractions on 13 kPa gels, but surprisingly evoked a more mixed effect on 1 kPa gels that did not reach statistical significance (Fig. 4B). Instead, time-lapse imaging on a 1 kPa gel revealed that cantharidin enhanced cell–matrix adhesion failure and cell retraction (Fig. 4C; see supplementary material Movie 3), suggesting that endogenous tension had in fact increased, but that adhesions failure was precluding a sustained increase in tractions on this soft matrix. Consistent with this interpretation, cantharidin treatment reduced 2D cell area on 1 kPa gels but not stiffer matrices (Fig. 4D), as did siRNA knockdown of the myosin-binding subunit of myosin phosphatase, MYPT1 (Fig. 4E), providing further evidence of an inverse relationship between actomyosin tension and cell spreading on soft matrices. Knockdown of MYPT1 also suppressed cell proliferation on 1 kPa gels with comparatively little effect on glass (Fig. 4F), recapitulating the stiffness-dependent effect of cantharidin. In agreement with the causal link between cell spreading and proliferation suggested above, cantharidin reduced cell proliferation rates as it reduced spreading, mirroring the ability of Rho–ROCK–myosin inhibition to promote cell spreading and proliferation on soft matrices. When plotted together, growth rates from the various matrix stiffness conditions at baseline and in the presence of Y27632 or cantharidin (Fig. 5A) collapsed onto a single curve, demonstrating a critical limiting role of 2D cell area on potential proliferation rate. This unifying observation was also observed when comparing the effects of knockdown of ROCK1+ROCK2, MYH9, or MYPT1 on cell area and proliferation on rigid and 1 kPa substrates (Fig. 5B). Together, these findings illustrate how manipulations of cytoskeletal tension and matrix stiffness shift cell behaviors along a master curve that relates cell proliferation to spreading.

Fig. 3. ROCK inhibition triggers cell spreading on soft matrices to promote proliferation. (**A**) Fibroblasts stained for F-actin (green) and nuclei (blue) across five stiffness conditions following 48 hours of exposure to no drug, blebbistatin (10 μM), or GSK429286 (1 μM). (**B**) Effect of matrix stiffness and Y27632 (10 μM) on 2D projected cell area. Means and individual data points ($n \geq 29$) are shown. Student's t-test: $^*P < 0.0001$ versus no drug. (**C**) Effect of combined ROCK1 and ROCK2 (ROCK1+2) siRNA knockdown and non-targeting [(−) control] siRNA on cell area. Means and individual data points ($n \geq 23$) are shown. Student's t-test: $^*P < 0.0001$ versus (−) control. (**D**) Fibroblasts on 1 kPa and rigid substrates were transfected with various concentrations of siRNA targeting both ROCK1 and ROCK2 and cultured for 6 days. Fold change in cell number is relative to the no siRNA condition for each stiffness condition. Means and individual data points ($n=3$) from one experiment are shown. (**E**) Fibroblasts across five stiffness conditions were transfected with 0.25 nM each of ROCK1 and ROCK2 siRNA and cultured for 6 days. For each stiffness condition, fold change in cell number is normalized to a 0.5 nM non-targeting siRNA control. Data are means ± s.d. ($n=6$). One-way ANOVA followed by Tukey's test: $^*P < 0.0001$ versus rigid (glass, G) condition. (**F**) Relationship between normalized cell proliferation and mean cell area with or without exposure to Y27632 (10 μM). (**G**) Time-lapse images of fibroblasts on a 1 kPa substrate following addition of Y27632 (10 μM) and subsequent washout. All images are at 200× magnification. Scale bar: 50 μm.

Discussion

Cells residing in soft matrix environments typically exhibit reduced proliferation or growth-arrest (Klein et al., 2009; Liu et al., 2010; Mih et al., 2011; Paszek et al., 2005; Tilghman et al., 2010; Ulrich et al., 2009). Many cellular features that are expressed on rigid substrates are also downregulated on soft matrices, including cell spreading, traction forces, myosin light chain phosphorylation, and focal adhesion assembly (Aratyn-Schaus and Gardel, 2010; Califano and Reinhart-King, 2010; Chowdhury et al., 2010; Fringer and Grinnell, 2001; Fu et al., 2010; Georges and Janmey, 2005; Ghosh et al., 2007; Kong et al., 2005; Levental et al., 2009; Lo et al., 2000; Paszek et al., 2005; Rhee et al., 2007; Saez et al., 2005; Solon et al., 2007; Wozniak et al., 2003). Because all of these features rise in concert with increasing matrix stiffness, each is suspected to play a positive role in the regulation of proliferation. However, on soft matrices ($E < 6$ kPa), we found that inhibiting actomyosin contractility led to a robust increase in proliferation (Fig. 1), in some cases rising to maximal proliferation rates attained on rigid substrates. The enhancement of cell proliferation simultaneous with suppression of cell tractions, p-MLC levels, and focal adhesions reveals that in this context, they are not fundamentally coupled with proliferation (Fig. 2). While this finding does not contradict the notion that some or all of these features may support or are necessary for proliferation in rigid environments (Assoian and Klein, 2008; Huang and Ingber, 1999; Mammoto and Ingber, 2009; Provenzano and Keely, 2011; Wozniak and Chen, 2009), they do demonstrate that such relationships break down on soft matrices.

In contrast, our results show that cell area remains tightly coupled with proliferation across wide variations in matrix stiffness and actomyosin contractility (Fig. 5A,B). Fibroblasts

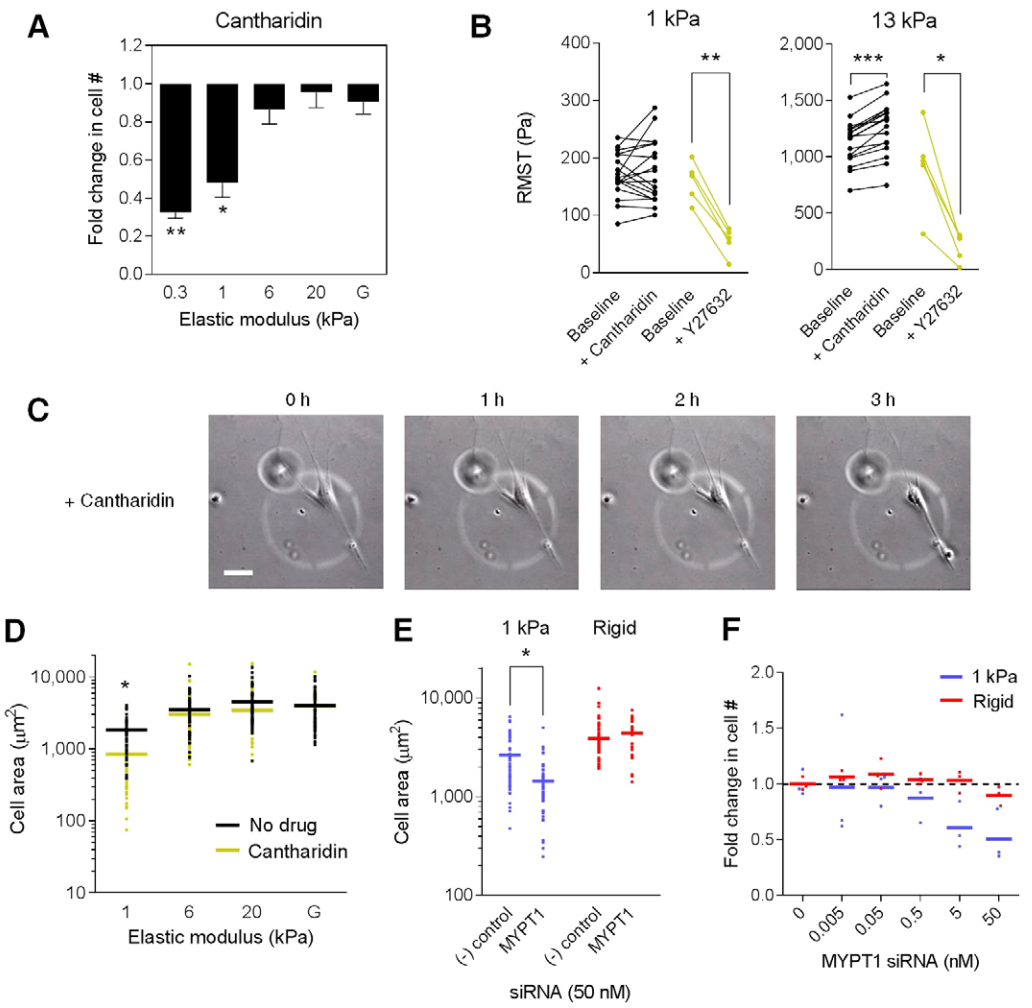

Fig. 4. Enhancing actomyosin tension leads to cell retraction and reduced proliferation on soft matrices. (**A**) Effect of cantharidin (1 μM) on cell proliferation across five stiffness conditions. Fold change indicates ratio of cell number in drug versus no drug samples after 72 hours. Data are means ± s.e.m. (n=5). One-way ANOVA followed by Tukey's test: *P<0.01, **P<0.0001 versus rigid (glass, G) condition. (**B**) RMST at baseline and following 2 hours of cantharidin (1 μM) or 45 minutes of Y27632 (10 μM) treatment. Paired observations of individual cells (cantharidin, n=17; Y27632, n=5) are connected. Paired t-test: *P=0.0059, **P=0.0002, ***P<0.0001 versus baseline RMST. (**C**) Time-lapse sequence of a fibroblast on a 1 kPa substrate following addition of cantharidin (0.3 μM). Images are at 200× magnification. Scale bar: 50 μm. (**D**) Effect of cantharidin (1 μM) on mean cell area (n≥29). One-way ANOVA followed by Tukey's test: *P<0.0001 versus rigid condition. (**E**) Effect of MYPT1 and non-targeting [(−) control] siRNA on cell area. Means and individual data points (n≥22) are shown. Student's t-test: *P<0.0001 versus (−) control. (**F**) Fibroblasts on 1 kPa and rigid substrates were transfected with siRNA targeting MYPT1 and cultured for 6 days. Fold change in cell number is relative to the no siRNA condition for each stiffness condition. Means and individual data points (n=3) from one experiment are shown.

transition from round to dendritic morphologies following inhibition of ROCK or myosin II (Fig. 3A,G), suggesting that the failure of cells to spread on soft matrices is due to a relative excess of actomyosin tension, not a lack thereof. Consistent with this explanation, we observed measurable cell tractions and phosphorylated myosin light chain on soft matrices that were attenuated by inhibition of ROCK (Fig. 2). Time-lapse imaging of the reversible and opposite effects of ROCK inhibition and cantharidin treatment on cell tractions and spreading offers further support for our conclusion that a matrix stiffness-dependent failure of cell–matrix adhesions underlies the restriction of cell spreading and proliferation on soft matrices. On rigid substrates, it is known that nascent adhesions normally grow and are reinforced under tension (Aratyn-Schaus and Gardel, 2010; Balaban et al., 2001; Galbraith et al., 2002; Geiger et al., 2009; Kuo et al., 2011). This process can be interrupted by Rho and ROCK inhibition, leading to adhesion disassembly. In contrast, our data suggest that on soft matrices, endogenous actomyosin-generated forces are too strong for nascent adhesions to persist or mature, limiting stable cell spreading. In the soft matrix context, ROCK inhibition appears to permit stable cell spreading through a mechanism that is independent of adhesion maturation (Galbraith et al., 2002; Pasapera et al., 2010), as we did not observe vinculin- or talin-positive focal adhesion assembly in cells that spread following ROCK inhibition (Fig. 2D,E). The soft matrix adhesions that form remain vulnerable, however, as ROCK inhibitor washout leads to adhesions failure rather than maturation (Aratyn-Schaus and Gardel, 2010), and cells revert to a rounded shape. Together, these observations suggest that the immature and transient nature

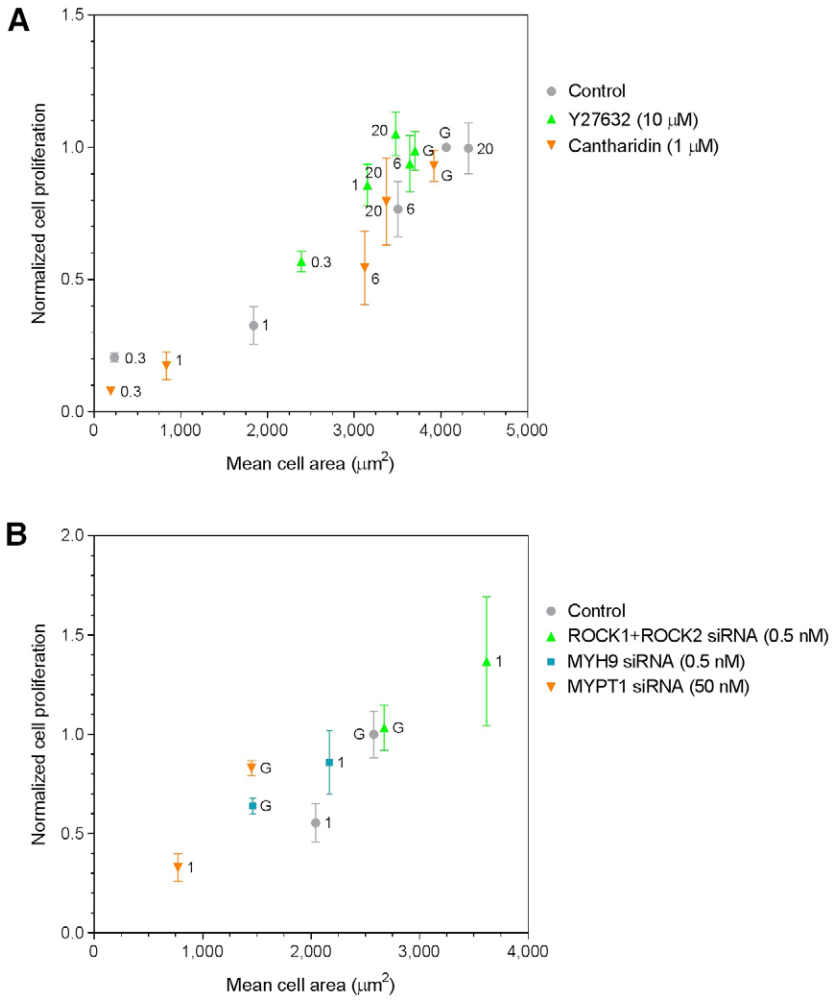

Fig. 5. Actomyosin tension and matrix stiffness converge on cell spreading to control proliferation. (**A**) Relationship between cell proliferation and area across five stiffness conditions. Proliferation is expressed as cell number relative to a control, rigid (glass, G) condition following 72 hours of culture. For Y27632 and cantharidin treatment conditions, data are proliferation means ± s.e.m. ($n \geq 4$) plotted against mean cell areas obtained in Fig. 3B and Fig. 4D. Elastic moduli (kPa) corresponding to each data point are indicated. (**B**) Effect of ROCK1+ROCK2, MYH9, and MYPT1 knockdown on cell area and proliferation. Cell numbers in soft (1 kPa) and rigid (G) conditions were determined 6 days following siRNA transfection. Proliferation is expressed as fold change in cell number relative to the rigid condition containing a matched concentration of non-targeting siRNA. Cell areas were determined 3 days following siRNA transfection. Data are proliferation means ± s.d. ($n=3$) plotted against mean cell areas from one representative experiment.

of adhesions on soft matrices is not due to a deficit in Rho-mediated tension, but on the contrary, arises from the inability of adhesions to reinforce and resist tension.

The robust relationship observed here between cell area and proliferation echoes previous observations of cell proliferation controlled by cell spreading (Chen et al., 1997; Folkman and Moscona, 1978). Similarly, the proliferative status of single endothelial cells can be predicted by nuclear volume, but not cell contractility (Roca-Cusachs et al., 2008). While the mechanism underlying shape-dependent control of cell proliferation is not known, our results are consistent with actomyosin tension acting upstream of cell shape to regulate proliferation on soft matrices, and not vice versa. They are also reminiscent of analogous relationships observed for other cell behaviors such as motility, where the same perturbation can have opposite effects on cells on soft versus stiff surfaces (Ulrich et al., 2009) or on low versus high matrix ligand densities (Palecek et al., 1997). In terms of mechanism, our preliminary efforts to identify cell cycle regulatory genes that control the stiffness-dependent growth effects of ROCK inhibition did not identify obvious candidates, indicating that more work will be needed to elucidate the underlying molecular network controlling this cellular response (supplementary material Table S1).

Taken together, our results demonstrate that a matrix stiffness-dependent balance between adhesions failure and reinforcement underlies a critical switch in Rho–ROCK–myosin effector functions. This switch occurs at an intermediate range of matrix stiffness (E ~ 6–20 kPa), where the effect of reducing cell tension on proliferation transitions from stimulatory to inhibitory. Below this threshold, cell shape and proliferation appear to be sensitively tuned to perturbations in actomyosin tension and matrix stiffness (Fig. 5). Because the range of matrix stiffness investigated here is relevant to a broad subset of human tissues, cellular processes, and disease conditions (Butcher et al., 2009; Discher et al., 2005; Guilak et al., 2009; Klein et al., 2009; Moore et al., 2010; Wozniak and Chen, 2009), these results may have important implications for our understanding of cell growth control in soft tissue environments.

Materials and Methods

Cell culture and assays

Primary normal human lung fibroblasts (Lonza) were used at passage 3–6. Primary human bone marrow-derived mesenchymal stem cells (Tulane University, USA) were used at passage 1–3, and human adipose-derived stem cells at passage 1–3 (ZenBio). All other cell types were obtained from ATCC. All cells were cultured in Kaighn's Modification of Ham's F12 Medium (F12K) supplemented with 10% fetal bovine serum, 100 U/ml penicillin and 100 μg/ml streptomycin (all from Cellgro) in a humidified 37℃ incubator with 5% CO_2. Y27632, GSK429286, cantharidin, and (+/−) blebbistatin were purchased from Tocris Bioscience, and cell-permeable C3 transferase obtained from Cytoskeleton. Unless otherwise indicated, cells were seeded in serum-free F12K media at 25 cells/mm^2 in multiwell plates containing polyacrylamide hydrogel substrates of defined stiffness. The hydrogels were cast and functionalized with collagen as

previously described (Mih et al., 2011). Four hours after seeding, media was replaced with F12K media with 10% serum and the indicated concentrations of drugs. Cell number was evaluated by Cyquant NF Cell Proliferation Assay (Life Technologies), which generates a fluorescent signal that is linearly correlated with cell number.

Traction microscopy

IMR-90 lung fibroblasts were used for all traction measurements. The cells were seeded at 10 cells/mm^2 on 0.3, 1, 6, and 20 kPa PA gels functionalized with collagen I (Purecol, Advanced Biomatrix). Fluorescent sulfate-modified microspheres, 0.2 μm in diameter, were attached to the gel surface and improved throughput traction microscopy (Marinković et al., 2012) was employed to capture the microsphere positions before and after removal of the cell by trypsinization. The pairs of fluorescent images were processed through a two-dimensional cross-correlation algorithm (Tolic-Norrelykke et al., 2002) to obtain the displacement field of the beads underneath the cell, and Fourier transform traction cytometry (Butler et al., 2002) was used to calculate the corresponding traction field generated by the cell on the gel surface. In order to compare measured traction fields, both in control and indicated treatment conditions, we computed root-mean-square tractions (RMSTs). The coordinates of the cell boundary required for traction calculation were obtained from the fluorescent images of the cell membrane (CellLight Plasma Membrane-RFP, Invitrogen) by applying a global threshold image processing algorithm (Marinković et al., 2012). All images were taken at 200× magnification. Cells were cultured on the gels for 24 hours prior to performing baseline traction measurements.

Immunofluorescence and cell area measurements

IMR-90 cells were seeded at 25 cells/mm^2 and cultured for 24 hours on PA gels or glass substrate. The cells were fixed in formalin, blocked with 10% normal goat serum in PBS for 1 hour, and permeabilized with 0.5% Triton X-100 in PBS for 5 minutes. The cells were incubated overnight with a mouse monoclonal antibody against vinculin (hVIN-1, Sigma), a mouse monoclonal antibody against talin (TLN01, sc-59882, Santa Cruz Biotechnologies), or a rabbit polyclonal antibody against phosphorylated myosin light chain 2 (S19, Cell Signaling Technologies), all diluted at 1:500. They were then washed 3× for 5 minutes each and incubated for 1 hour with a secondary goat anti-mouse (or rabbit) AlexaFlour 488-conjugated antibody (Life Technologies) diluted 1:500 in PBS, and washed 3× prior to fluorescence imaging. For measurements of cell area, fixed cells were stained with Alexafluor 586-phalloidin and Hoechst (Life Technologies), and fluorescent images were analyzed by CellProfiler (Broad Institute) to calculate 2D projected cell area based on F-actin staining. Focal adhesion morphometry was analyzed by established methods (Dugina et al., 2001) using MetaMorph 6 software. The length of stained FAs was defined by their longest axis in the direction of lamellar spreading and was measured within the lamellar zone of cell edge (Fig. 2B).

RNA interference

IMR-90 cells were transfected using Lipofectamine RNAiMAX (Life Technologies) with an siRNA SMARTpool (Thermo Scientific) containing four siRNAS targeting human MYH9, ROCK1, ROCK2, MYPT1, or a non-targeting SMARTpool (see supplementary material Table S2 for siRNA sequences). Cells were seeded onto 1 kPa or rigid substrates and exposed to 0.005, 0.05, 0.5, 5, or 50 nM of targeting or non-targeting siRNA. For simultaneous knockdown of ROCK1 and ROCK2, equivalent amounts of each siRNA were added to reach the indicated concentration. Media was replaced after 8 hours and cells were cultured for 6 days. Cell number was determined using the Cyquant assay. Knockdown of each siRNA target was confirmed by western blot following 72 hours of transfection using 1:1000 dilutions of rabbit antibodies against MYH9, ROCK1, MYPT (Cell Signaling Technologies), and ROCK2 (Santa Cruz Biotechnology). Chemiluminescence-based detection was performed using a 1:2000 dilution of secondary HRP-linked goat anti-rabbit antibody (Cell Signaling Technologies) followed by exposure to SuperSignal West Femto Substrate (Thermo Scientific) and imaging with a high-resolution CCD camera (Syngene).

3D culture

IMR-90 cells were mixed with Geltrex reduced growth factor basement membrane extract (Life Technologies) at 1 part cell solution to 9 parts Geltrex and at a final density of 50,000 cells/ml. 50 μl of the mixture was delivered to individual wells of a non-TC-treated, 96-well polystyrene plate and allowed to gel for one hour at 37℃. The hydrogels were overlaid with media and incubated for 4 hours prior to addition of ROCK inhibitors. The number of cells after 5 days of culture relative to the initial seeding density at 4 hours was determined using a cell counting kit (Donjindo) based on the colorimetric detection of formazan. The number of cells attaching to the rigid well bottom was negligible under all conditions.

PCR array

IMR-90 fibroblasts were seeded at subconfluency on 1 kPa and glass substrates and cultured for 24 hours in F12K media containing 10% FBS. Cells in each condition were then exposed to 10 μM Y27632 or no treatment for 12 hours. Total RNA was isolated using a spin-column based kit (RNeasy, Qiagen) with DNase I digestion. RNA (100 ng) was reverse transcribed to cDNA (RT^2 First Strand Kit, Qiagen), combined with RT^2 SYBR Green qPCR Mastermix (Qiagen), and delivered to a 96-well, Human Cell Cycle PCR Array (Qiagen). The array was subject to 95℃ for 10 minutes, then 40 cycles of 95℃ for 15 seconds and 60℃ for 1 minute using a real-time PCR cycler (Applied Biosystems Model 7300).

Funding

This work was supported by the National Institutes of Health [grant numbers HL-092961, T32-HL-007118]. Deposited in PMC for release after 12 months.

Supplementary material available online at
http://jcs.biologists.org/lookup/suppl/doi:10.1242/jcs.108886/-/DC1

References

Aratyn-Schaus, Y. and Gardel, M. L. (2010). Transient frictional slip between integrin and the ECM in focal adhesions under myosin II tension. *Curr. Biol.* **20**, 1145-1153.

Assoian, R. K. and Klein, E. A. (2008). Growth control by intracellular tension and extracellular stiffness. *Trends Cell Biol.* **18**, 347-352.

Balaban, N. Q., Schwarz, U. S., Riveline, D., Goichberg, P., Tzur, G., Sabanay, I., Mahalu, D., Safran, S., Bershadsky, A., Addadi, L. et al. (2001). Force and focal adhesion assembly: a close relationship studied using elastic micropatterned substrates. *Nat. Cell Biol.* **3**, 466-472.

Butcher, D. T., Alliston, T. and Weaver, V. M. (2009). A tense situation: forcing tumour progression. *Nat. Rev. Cancer* **9**, 108-122.

Butler, J. P., Tolić-Nørrelykke, I. M., Fabry, B. and Fredberg, J. J. (2002). Traction fields, moments, and strain energy that cells exert on their surroundings. *Am. J. Physiol. Cell Physiol.* **282**, C595-C605.

Cai, Y., Biais, N., Giannone, G., Tanase, M., Jiang, G., Hofman, J. M., Wiggins, C. H., Silberzan, P., Buguin, A., Ladoux, B. et al. (2006). Nonmuscle myosin IIA-dependent force inhibits cell spreading and drives F-actin flow. *Biophys. J.* **91**, 3907-3920.

Califano, J. P. and Reinhart-King, C. A. (2010). Substrate stiffness and cell area predict cellular traction stresses in single cells and cells in contact. *Cell Mol. Bioeng.* **3**, 68-75.

Chen, C. S., Mrksich, M., Huang, S., Whitesides, G. M. and Ingber, D. E. (1997). Geometric control of cell life and death. *Science* **276**, 1425-1428.

Chicurel, M. E., Chen, C. S. and Ingber, D. E. (1998). Cellular control lies in the balance of forces. *Curr. Opin. Cell Biol.* **10**, 232-239.

Chowdhury, F., Li, Y., Poh, Y. C., Yokohama-Tamaki, T., Wang, N. and Tanaka, T. S. (2010). Soft substrates promote homogeneous self-renewal of embryonic stem cells via downregulating cell-matrix tractions. *PLoS ONE* **5**, e15655.

Discher, D. E., Janmey, P. and Wang, Y. L. (2005). Tissue cells feel and respond to the stiffness of their substrate. *Science* **310**, 1139-1143.

Dugina, V., Fontao, L., Chaponnier, C., Vasiliev, J. and Gabbiani, G. (2001). Focal adhesion features during myofibroblastic differentiation are controlled by intracellular and extracellular factors. *J. Cell Sci.* **114**, 3285-3296.

Folkman, J. and Moscona, A. (1978). Role of cell shape in growth control. *Nature* **273**, 345-349.

Fringer, J. and Grinnell, F. (2001). Fibroblast quiescence in floating or released collagen matrices: contribution of the ERK signaling pathway and actin cytoskeletal organization. *J. Biol. Chem.* **276**, 31047-31052.

Fu, J., Wang, Y. K., Yang, M. T., Desai, R. A., Yu, X., Liu, Z. and Chen, C. S. (2010). Mechanical regulation of cell function with geometrically modulated elastomeric substrates. *Nat. Methods* **7**, 733-736.

Galbraith, C. G., Yamada, K. M. and Sheetz, M. P. (2002). The relationship between force and focal complex development. *J. Cell Biol.* **159**, 695-705.

Geiger, B., Spatz, J. P. and Bershadsky, A. D. (2009). Environmental sensing through focal adhesions. *Nat. Rev. Mol. Cell Biol.* **10**, 21-33.

Georges, P. C. and Janmey, P. A. (2005). Cell type-specific response to growth on soft materials. *J. Appl. Physiol.* **98**, 1547-1553.

Ghosh, K., Pan, Z., Guan, E., Ge, S., Liu, Y., Nakamura, T., Ren, X. D., Rafailovich, M. and Clark, R. A. (2007). Cell adaptation to a physiologically relevant ECM mimic with different viscoelastic properties. *Biomaterials* **28**, 671-679.

Grinnell, F., Ho, C. H., Tamariz, E., Lee, D. J. and Skuta, G. (2003). Dendritic fibroblasts in three-dimensional collagen matrices. *Mol. Biol. Cell* **14**, 384-395.

Guilak, F., Cohen, D. M., Estes, B. T., Gimble, J. M., Liedtke, W. and Chen, C. S. (2009). Control of stem cell fate by physical interactions with the extracellular matrix. *Cell Stem Cell* **5**, 17-26.

Guo, W. H., Frey, M. T., Burnham, N. A. and Wang, Y. L. (2006). Substrate rigidity regulates the formation and maintenance of tissues. *Biophys. J.* **90**, 2213-2220.

Hotulainen, P. and Lappalainen, P. (2006). Stress fibers are generated by two distinct actin assembly mechanisms in motile cells. *J. Cell Biol.* **173**, 383-394.

Huang, S., Chen, C. S. and Ingber, D. E. (1998). Control of cyclin D1, p27(Kip1), and cell cycle progression in human capillary endothelial cells by cell shape and cytoskeletal tension. *Mol. Biol. Cell* **9**, 3179-3193.

Huang, S. and Ingber, D. E. (1999). The structural and mechanical complexity of cell-growth control. *Nat. Cell Biol.* **1**, E131-E138.

Klein, E. A., Yin, L., Kothapalli, D., Castagnino, P., Byfield, F. J., Xu, T., Levental, I., Hawthorne, E., Janmey, P. A. and Assoian, R. K. (2009). Cell-cycle control by physiological matrix elasticity and in vivo tissue stiffening. *Curr. Biol.* **19**, 1511-1518.

Knapp, J., Bokník, P., Huke, S., Lüss, H., Müller, F. U., Müller, T., Nacke, P., Schmitz, W., Vahlensieck, U. and Neumann, J. (1998). The mechanism of action of cantharidin in smooth muscle. *Br. J. Pharmacol.* **123**, 911-919.

Kong, H. J., Polte, T. R., Alsberg, E. and Mooney, D. J. (2005). FRET measurements of cell-traction forces and nano-scale clustering of adhesion ligands varied by substrate stiffness. *Proc. Natl. Acad. Sci. USA* **102**, 4300-4305.

Kuo, J. C., Han, X., Hsiao, C. T., Yates, J. R., 3rd and Waterman, C. M. (2011). Analysis of the myosin-II-responsive focal adhesion proteome reveals a role for β-Pix in negative regulation of focal adhesion maturation. *Nat. Cell Biol.* **13**, 383-393.

Levental, K. R., Yu, H., Kass, L., Lakins, J. N., Egeblad, M., Erler, J. T., Fong, S. F., Csiszar, K., Giaccia, A., Weninger, W. et al. (2009). Matrix crosslinking forces tumor progression by enhancing integrin signaling. *Cell* **139**, 891-906.

Liu, F., Mih, J. D., Shea, B. S., Kho, A. T., Sharif, A. S., Tager, A. M. and Tschumperlin, D. J. (2010). Feedback amplification of fibrosis through matrix stiffening and COX-2 suppression. *J. Cell Biol.* **190**, 693-706.

Lo, C. M., Wang, H. B., Dembo, M. and Wang, Y. L. (2000). Cell movement is guided by the rigidity of the substrate. *Biophys. J.* **79**, 144-152.

Mammoto, A., Huang, S., Moore, K., Oh, P. and Ingber, D. E. (2004). Role of RhoA, mDia, and ROCK in cell shape-dependent control of the Skp2-p27kip1 pathway and the G1/S transition. *J. Biol. Chem.* **279**, 26323-26330.

Mammoto, A. and Ingber, D. E. (2009). Cytoskeletal control of growth and cell fate switching. *Curr. Opin. Cell Biol.* **21**, 864-870.

Marinković, A., Mih, J. D., Park, J. A., Liu, F. and Tschumperlin, D. J. (2012). Improved throughput traction microscopy reveals pivotal role for matrix stiffness in fibroblast contractility and TGF-β responsiveness. *Am. J. Physiol. Lung Cell. Mol. Physiol.* **303**, L169-L180.

McBeath, R., Pirone, D. M., Nelson, C. M., Bhadriraju, K. and Chen, C. S. (2004). Cell shape, cytoskeletal tension, and RhoA regulate stem cell lineage commitment. *Dev. Cell* **6**, 483-495.

Mih, J. D., Sharif, A. S., Liu, F., Marinkovic, A., Symer, M. M. and Tschumperlin, D. J. (2011). A multiwell platform for studying stiffness-dependent cell biology. *PLoS ONE* **6**, e19929.

Moore, S. W., Roca-Cusachs, P. and Sheetz, M. P. (2010). Stretchy proteins on stretchy substrates: the important elements of integrin-mediated rigidity sensing. *Dev. Cell* **19**, 194-206.

Palecek, S. P., Loftus, J. C., Ginsberg, M. H., Lauffenburger, D. A. and Horwitz, A. F. (1997). Integrin-ligand binding properties govern cell migration speed through cell-substratum adhesiveness. *Nature* **385**, 537-540.

Pasapera, A. M., Schneider, I. C., Rericha, E., Schlaepfer, D. D. and Waterman, C. M. (2010). Myosin II activity regulates vinculin recruitment to focal adhesions through FAK-mediated paxillin phosphorylation. *J. Cell Biol.* **188**, 877-890.

Paszek, M. J., Zahir, N., Johnson, K. R., Lakins, J. N., Rozenberg, G. I., Gefen, A., Reinhart-King, C. A., Margulies, S. S., Dembo, M., Boettiger, D. et al. (2005). Tensional homeostasis and the malignant phenotype. *Cancer Cell* **8**, 241-254.

Provenzano, P. P. and Keely, P. J. (2011). Mechanical signaling through the cytoskeleton regulates cell proliferation by coordinated focal adhesion and Rho GTPase signaling. *J. Cell Sci.* **124**, 1195-1205.

Rhee, S., Jiang, H., Ho, C. H. and Grinnell, F. (2007). Microtubule function in fibroblast spreading is modulated according to the tension state of cell-matrix interactions. *Proc. Natl. Acad. Sci. USA* **104**, 5425-5430.

Roca-Cusachs, P., Alcaraz, J., Sunyer, R., Samitier, J., Farré, R. and Navajas, D. (2008). Micropatterning of single endothelial cell shape reveals a tight coupling between nuclear volume in G1 and proliferation. *Biophys. J.* **94**, 4984-4995.

Saez, A., Buguin, A., Silberzan, P. and Ladoux, B. (2005). Is the mechanical activity of epithelial cells controlled by deformations or forces? *Biophys. J.* **89**, L52-L54.

Shin, J. W., Swift, J., Spinler, K. R. and Discher, D. E. (2011). Myosin-II inhibition and soft 2D matrix maximize multinucleation and cellular projections typical of platelet-producing megakaryocytes. *Proc. Natl. Acad. Sci. USA* **108**, 11458-11463.

Solon, J., Levental, I., Sengupta, K., Georges, P. C. and Janmey, P. A. (2007). Fibroblast adaptation and stiffness matching to soft elastic substrates. *Biophys. J.* **93**, 4453-4461.

Straight, A. F., Cheung, A., Limouze, J., Chen, I., Westwood, N. J., Sellers, J. R. and Mitchison, T. J. (2003). Dissecting temporal and spatial control of cytokinesis with a myosin II Inhibitor. *Science* **299**, 1743-1747.

Tilghman, R. W., Cowan, C. R., Mih, J. D., Koryakina, Y., Gioeli, D., Slack-Davis, J. K., Blackman, B. R., Tschumperlin, D. J. and Parsons, J. T. (2010). Matrix rigidity regulates cancer cell growth and cellular phenotype. *PLoS ONE* **5**, e12905.

Tolić-Nørrelykke, I. M. and Wang, N. (2005). Traction in smooth muscle cells varies with cell spreading. *J. Biomech.* **38**, 1405-1412.

Tolić-Nørrelykke, I. M., Butler, J. P., Chen, J. and Wang, N. (2002). Spatial and temporal traction response in human airway smooth muscle cells. *Am. J. Physiol., Cell Physiol.* **283**. doi: 10.1152/ajpcell.00169.2002

Ulrich, T. A., de Juan Pardo, E. M. and Kumar, S. (2009). The mechanical rigidity of the extracellular matrix regulates the structure, motility, and proliferation of glioma cells. *Cancer Res.* **69**, 4167-4174.

Wang, N., Ostuni, E., Whitesides, G. M. and Ingber, D. E. (2002). Micropatterning tractional forces in living cells. *Cell Motil. Cytoskeleton* **52**, 97-106.

Wozniak, M. A. and Chen, C. S. (2009). Mechanotransduction in development: a growing role for contractility. *Nat. Rev. Mol. Cell Biol.* **10**, 34-43.

Wozniak, M. A., Desai, R., Solski, P. A., Der, C. J. and Keely, P. J. (2003). ROCK-generated contractility regulates breast epithelial cell differentiation in response to the physical properties of a three-dimensional collagen matrix. *J. Cell Biol.* **163**, 583-595.

Journal of Cell Science

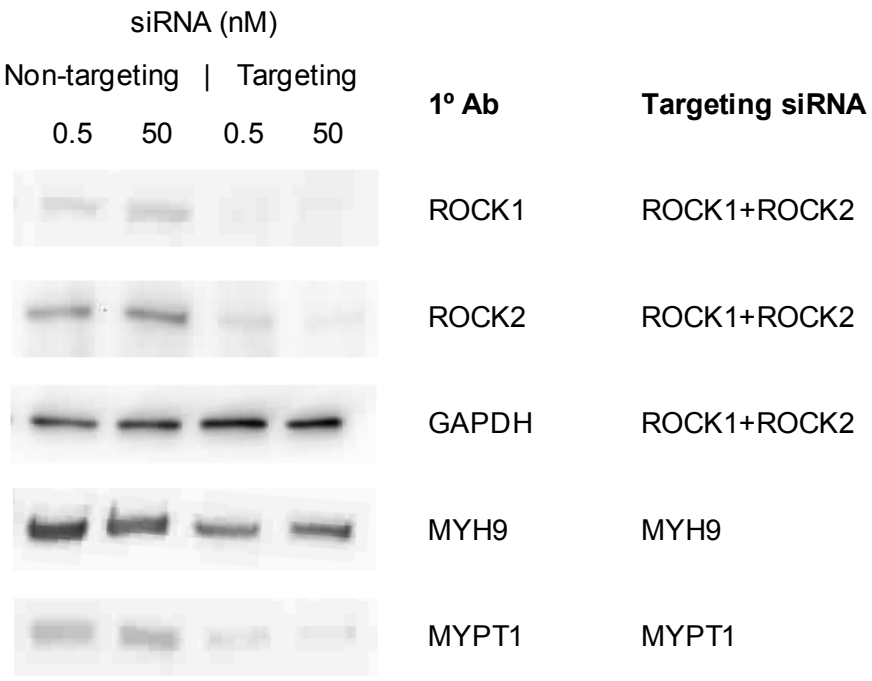

Fig. S1. Western blotting evaluation of siRNA knockdown. Fibroblasts grown on rigid (glass) substrates were transfected with the indicated concentrations of non-targeting or targeting siRNA. Similar siRNA knockdown efficacy is observed on soft hydrogels (data not shown). For ROCK1+ROCK2 co-transfections, 0.25 or 25 nM of each siRNA was used. Protein was isolated 72 hours after transfection. GAPDH serves as a loading control for the non-targeting and ROCK1+ROCK2 conditions.

Movie 1. Phase contrast image sequence of IMR-90 fibroblasts on a 1 kPa substrate before and after addition of 10 μM Y27632 (at frame 31, 2 sec).

Movie 2. Phase contrast image sequence of IMR-90 fibroblasts following washout of Y27632. Images were acquired at 2 min intervals, 200x magnification, and compiled at 15 frames/sec.

Movie 3. Phase contrast image sequence of IMR-90 fibroblasts on a 1 kPa substrate after addition of 0.3 μM cantharidin. Images were acquired at 10 min intervals, 200x magnification, and compiled at 2 frames/sec.

Table S1. Profile of cell cycle gene expression in IMR-90 fibroblasts. For each condition, changes in transcript levels are normalized to a panel of housekeeping genes, and then expressed relative to the 1 kPa, no treatment control.

Symbol	Description	1 kPa	1 kPa + Y27632	Rigid	Rigid +Y27632
ABL1	C-abl oncogene 1, non-receptor tyrosine kinase	1	0.485	1.0345	0.6522
ANAPC2	Anaphase promoting complex subunit 2	1	0.4412	1.178	1.1432
ATR	Ataxia telangiectasia and Rad3 related	1	0.6424	0.5195	0.5656
AURKA	Aurora kinase A	1	0.5688	0.9732	0.6778
AURKB	Aurora kinase B	1	0.7715	0.5515	0.7635
BCCIP	BRCA2 and CDKN1A interacting protein	1	0.4579	1.4387	1.4579
BCL2	B-cell CLL/lymphoma 2	1	0.9058	0.8427	0.6226
BIRC5	Baculoviral IAP repeat containing 5	1	0.7923	1.447	1.3317
BRCA1	Breast cancer 1, early onset	1	0.8837	1.0382	0.7845
BRCA2	Breast cancer 2, early onset	1	0.709	1.2939	1.078
CASP3	Caspase 3, apoptosis-related cysteine peptidase	1	0.6996	1.6761	0.8295
CCNA2	Cyclin A2	1	0.9015	1.3686	0.8332
CCNB1	Cyclin B1	1	1.0724	1.2683	0.8197
CCNB2	Cyclin B2	1	0.9239	1.2286	0.7428
CCNC	Cyclin C	1	0.6458	1.5687	1.3432
CCND1	Cyclin D1	1	0.9607	1.8183	1.283
CCND2	Cyclin D2	1	0.3938	1.3734	0.7584
CCND3	Cyclin D3	1	0.3481	2.5126	1.8493
CCNE1	Cyclin E1	1	1.0795	1.1718	0.9893
CCNF	Cyclin F	1	0.8067	0.9553	0.9025
CCNG1	Cyclin G1	1	0.8925	1.0701	0.7013
CCNG2	Cyclin G2	1	0.505	1.2193	0.704
CCNH	Cyclin H	1	0.5612	0.7453	0.5837
CCNT1	Cyclin T1	1	0.9036	0.7322	0.5243
CDC16	Cell division cycle 16 homolog (S. cerevisiae)	1	1.1951	1.8278	0.8269
CDC20	Cell division cycle 20 homolog (S. cerevisiae)	1	0.6473	1.2699	0.8903
CDC25A	Cell division cycle 25 homolog A (S. pombe)	1	0.3856	1.3874	1.0553
CDC25C	Cell division cycle 25 homolog C (S. pombe)	1	0.9675	0.9028	0.6351
CDC34	Cell division cycle 34 homolog (S. cerevisiae)	1	0.9291	0.9389	0.6426
CDC6	Cell division cycle 6 homolog (S. cerevisiae)	1	0.3727	1.2094	0.5952
CDK1	Cyclin-dependent kinase 1	1	0.5083	1.0164	0.8214
CDK2	Cyclin-dependent kinase 2	1	0.4739	1.2037	0.6686
CDK4	Cyclin-dependent kinase 4	1	0.7919	0.9038	0.5471
CDK5R1	Cyclin-dependent kinase 5, regulatory subunit 1 (p35)	1	0.8243	0.9794	0.5834
CDK5RAP1	CDK5 regulatory subunit associated protein 1	1	0.7477	0.8799	0.5438
CDK6	Cyclin-dependent kinase 6	1	0.6167	1.7037	1.485
CDK7	Cyclin-dependent kinase 7	1	1.1416	1.0338	1.0919
CDK8	Cyclin-dependent kinase 8	1	0.9365	1.0323	0.658
CDKN1A	Cyclin-dependent kinase inhibitor 1A (p21, Cip1)	1	0.8961	1.9026	1.2463
CDKN1B	Cyclin-dependent kinase inhibitor 1B (p27, Kip1)	1	0.8755	1.0965	0.7509
CDKN2A	Cyclin-dependent kinase inhibitor 2A (melanoma, p16, inhibits CDK4)	1	0.7876	0.9557	0.5916
CDKN2B	Cyclin-dependent kinase inhibitor 2B (p15, inhibits CDK4)	1	1.0204	1.2935	1.0065
CDKN3	Cyclin-dependent kinase inhibitor 3	1	0.8378	1.5588	1.1824
CHEK1	CHK1 checkpoint homolog (S. pombe)	1	0.8634	0.8742	0.7349
CKS1B	CDC28 protein kinase regulatory subunit 1B	1	0.8844	0.7246	0.6131
CKS2	CDC28 protein kinase regulatory subunit 2	1	0.3982	1.1877	1.0142

CUL2	Cullin 2	1	1.0267	0.9997	0.9892
E2F1	E2F transcription factor 1	1	0.9856	1.1033	0.7181
E2F4	E2F transcription factor 4, p107/p130-binding	1	0.8477	1.3832	0.9555
GADD45A	Growth arrest and DNA-damage-inducible, alpha	1	1.1697	1.0231	0.8399
GTSE1	G-2 and S-phase expressed 1	1	0.7593	1.44	0.9906
HUS1	HUS1 checkpoint homolog (S. pombe)	1	0.8684	0.7826	0.5811
KNTC1	Kinetochore associated 1	1	0.6607	0.9556	0.606
KPNA2	Karyopherin alpha 2 (RAG cohort 1, importin alpha 1)	1	0.8675	1.4081	1.0181
MAD2L1	MAD2 mitotic arrest deficient-like 1 (yeast)	1	0.4383	1.5059	1.2541
MAD2L2	MAD2 mitotic arrest deficient-like 2 (yeast)	1	0.1298	1.4487	1.3456
MCM2	Minichromosome maintenance complex component 2	1	0.5905	1.0974	0.7266
MCM3	Minichromosome maintenance complex component 3	1	0.5879	1.4588	0.9143
MCM4	Minichromosome maintenance complex component 4	1	0.4273	1.089	0.8579
MCM5	Minichromosome maintenance complex component 5	1	0.5808	1.6935	0.8643
MDM2	Mdm2 p53 binding protein homolog (mouse)	1	0.8872	1.0891	0.5905
MKI67	Antigen identified by monoclonal antibody Ki-67	1	0.5137	1.4869	1.497
MNAT1	Menage a trois homolog 1, cyclin H assembly factor (Xenopus laevis)	1	0.7794	1.0918	0.7652
MRE11A	MRE11 meiotic recombination 11 homolog A (S. cerevisiae)	1	1.6962	2.4657	1.5792
NBN	Nibrin	1	0.9891	0.7195	0.5762
RAD1	RAD1 homolog (S. pombe)	1	0.9127	0.757	0.6637
RAD17	RAD17 homolog (S. pombe)	1	0.974	0.9555	0.8911
RAD51	RAD51 homolog (S. cerevisiae)	1	0.4441	0.7951	0.7601
RAD9A	RAD9 homolog A (S. pombe)	1	0.9363	1.6467	0.9611
RB1	Retinoblastoma 1	1	1.1108	1.2121	0.706
RBBP8	Retinoblastoma binding protein 8	1	0.6596	1.2618	0.9633
RBL1	Retinoblastoma-like 1 (p107)	1	0.9453	0.8861	1.0161
RBL2	Retinoblastoma-like 2 (p130)	1	0.8969	1.1147	0.8919
SERTAD1	SERTA domain containing 1	1	0.4999	0.8991	0.6486
SKP2	S-phase kinase-associated protein 2 (p45)	1	0.7572	1.2387	0.7905
STMN1	Stathmin 1	1	0.9171	0.9505	0.7916
TFDP1	Transcription factor Dp-1	1	0.4876	1.5845	1.3417
TFDP2	Transcription factor Dp-2 (E2F dimerization partner 2)	1	0.8007	0.8305	0.6302
TP53	Tumor protein p53	1	0.6244	2.0388	1.5771
WEE1	WEE1 homolog (S. pombe)	1	0.3332	1.1666	1.2536

Table S2. siRNA sequences.

Non-targeting
Duplex #1: 5'-UGGUUUACAUGUCGACUAA-3’
Duplex #2: 5'-UGGUUUACAUGUUGUGUGA-3’
Duplex #3: 5'-UGGUUUACAUGUUUUCUGA-3’
Duplex #4: 5'-UGGUUUACAUGUUUUCCUA-3’

Target: *MYH9*
Duplex #5: 5’-GUAUCAAUGUGACCGAUUU-3’
Duplex #6: 5’-CAAAGGAGCCCUGGCGUUA-3’
Duplex #7: 5’-GGAGGAACGCCGAGCAGUA-3’
Duplex #8: 5’-CGAAGCGGGUGAAAGCAAA-3’

Target: *MYPT1*
Duplex #7: 5’-CAACUAAACAGGCCAAAUA-3’
Duplex #8: 5’-GCUAAAUAGUGGUCAUAUA-3’
Duplex #9: 5’-ACAAAGAGACGUUGAUUAU-3’
Duplex #10: 5’-CGGAUUCCAUUUCUAGAUA-3’

Target: *ROCK1*
Duplex #6: 5’-CUACAAGUGUUGCUAGUUU-3’
Duplex #7: 5’-UAGCAAUCGUAGAUACUUA-3’
Duplex #8: 5’-CCAGGAAGGUAUAUGCUAU-3’
Duplex #9: 5’-GCCAAUGACUUACUUAGGA-3’

Target: *ROCK2*
Duplex #6: 5’-GCAACUGGCUCGUUCAAUU-3’
Duplex #7: 5’-UAGAAUAUGUGGCCUAGAA-3’
Duplex #8: 5’-GAAACUAAUAGGACACUAA-3’
Duplex #9: 5’-CAAACUUGGUAAAGAAUUG-3’